The Stabilization of Spreading Shear Faults by Coupled Deformation-Diffusion Effects in Fluid-Infiltrated Porous Materials

JAMES R. RICE AND DONALD A. SIMONS

Division of Engineering, Brown University, Providence, Rhode Island 02912

A mathematical solution is developed for the steady, quasi-static, plane strain advance of a shear fault in a fluid-infiltrated elastic porous material. As revealed through analysis of some elementary fracture mechanics models, the coupled deformation-diffusion effects in such a material lead to a required 'force' to drive the fault that increases continuously with fault velocity up to a maximum value. The nominal fault tip energy release rate required for spreading at this maximum is greater than that for very slow speeds by a factor approaching $(1 - \nu)^2/(1 - \nu_u)^2$, where ν and ν_u are the elastic Poisson's ratios under 'drained' and 'undrained' conditions, respectively. The effect is numerically significant and provides a mechanism by which a spreading shear fault can, within limits, be stabilized against catastrophic (seismic) propagation. Predictions of the model are compared to data representative of creep events on the San Andreas system. It is concluded that the speeds and slipping lengths of the observed events are consistent with their being stabilized by the effect discussed, and hence the model would seem to provide a viable mechanism for fault creep. Similar effects may be operative also in setting the time scale of progressive landslide failures in overconsolidated clay soils, in which rupture occurs by propagation of a narrow slip surface.

INTRODUCTION

A fluid-infiltrated, porous elastic material responds to time-varying loadings in a manner that is more or less stiff depending on the time scale of the loading. If load variations are rapid enough to preclude diffusive transport of pore fluid over the time span of interest, the material will behave as though 'undrained' and will appear to be relatively stiff in comparison with the case where the time scale is long enough to allow 'drained' response, with diffusive dissipation of any induced pore pressures. This means that the concentration of stresses near the tip of a spreading shear fault in such a medium will depend on the rate of spreading and consequently, in fracture mechanics terminology, that more energy can be released to breakdown processes at the edge of the fault during slow (drained) than during fast (undrained) spreading (see *Rice and Cleary* [1976], henceforth abbreviated RC).

By solving mathematically the steady state, plane strain problem of a quasi-statically advancing shear fault in a porous elastic solid, we shall demonstrate directly that the coupled deformation-diffusion effects alluded to in the foregoing do in fact lead to a speed-dependent stress concentration at the fault tip. Further, upon introduction of a simple rupture model, involving a zone of degrading shear strength near the fault tip, we are able to calculate the applied stress necessary to drive the fault at any given speed. The required driving stress is found to increase with speed to a maximum value, at which the nominal crack extension force required for fault spreading has increased by a factor between β and β^2 times its value for low-speed (drained) conditions, where $\beta \equiv (1 - \nu)/(1 - \nu_u) > 1$, and ν, ν_u are the elastic Poisson's ratios of the fluid-infiltrated rock under drained and undrained conditions, respectively.

This effect seems to be numerically significant and may well contribute to the stabilization of earth fault slippage events against rapid propagation. As such, the model provides a description of a possible mechanism for fault creep.

Indeed, observations of creep events [e.g., *Scholz et al.*, 1969; *King et al.*, 1973] suggest that these consist of the stable, essentially quasi-static, episodic propagation of slip offsets along existing faults. The apparent fault spreading speeds are many orders of magnitude less than those under seismic conditions and cover a range typically from 1 to 10 km/d, although one apparent speed reported by the latter workers was as high as 80 km/d. Any proposed mechanism for this sort of behavior should entail a driving stress for fault propagation which increases monotonically with spreading speed over the above range. Otherwise, small perturbations in the spreading speed would lead to very rapid (seismic) propagation, rather than the observed quasi-static motion. As suggested by the preliminary analysis in RC and confirmed by our detailed analysis here, the model under discussion, based on porous media effects, does seem to be consistent with this requirement. Further, there is some evidence [*Johnson et al.*, 1974], based on water level changes in deep wells, for transient pore pressure alterations of the type anticipated here in association with creep events.

This does not, of course, eliminate other mechanisms as possible contributors to the stabilization of fault creep. Nor does it eliminate the ancillary requirement for stable fractional sliding, as opposed to stick slip, to be possible over the corresponding range of slippage velocities in order for creep events to occur as such [*Scholz et al.*, 1969].

Palmer and Rice [1973] (henceforth abbreviated PR) and *Rice* [1973] have discussed some other possible mechanisms for stabilization in connection with the spreading of narrow shear rupture zones (or 'slip surfaces') in landslides and other failures of overconsolidated clay soils [e.g., *Skempton*, 1964; *Bjerrum*, 1967], but these may be equally applicable to fault creep. They include (i) viscoelastic material behavior, which may be due to a secondary-consolidationlike creep in clay or to an apparent creep in stressed rock owing to the corrosive growth of microcracks [*Scholz*, 1968]; (ii) the 'effective stress' based increase in fracture energy due to pore-fluid suctions, induced transiently, by prefailure dilatant deformation in the breakdown zone at the spreading edge of a fault (see also RC for a discussion relating to faults in rock); and (iii) any rheological factors which could serve to give an increasing frictional resistance, with slippage speed, to the adjoining fault surfaces or possibly to the deforming fault gouge between them. (In this

connection, *Nason and Weertman* [1973] suggest the necessity of an upper yield point behavior in the fault gouge.)

The organization of the paper is as follows: In the next section we discuss some concepts from the fracture mechanics of shear cracks in 'elastic' bodies (i.e., bodies obeying the equations of classical elasticity, as contrasted with fluid-infiltrated, porous, elastic bodies, which we refer to subsequently as 'porous elastic' for brevity). These fracture mechanics concepts are directly applicable to porous elastic media in the long- and short-time (drained and undrained) limits because in these limits a porous elastic material behaves as an elastic material of the same shear modulus G and Poisson's ratio ν_e equal, respectively, to the drained or undrained ratio, ν or ν_u. Moreover, the topics presented provide the framework for much of the analysis and discussion to follow.

Next, the coupled deformation-diffusion equations governing quasi-static plane strain of a fluid-infiltrated porous elastic medium are given. Then, in order to illustrate most simply the effects under consideration, these equations are solved for the simple case of a semi-infinite shear crack (or fault) advancing quasi-statically at a uniform speed V such that the deformation field is fixed relative to an observer advancing with the fault. This is followed by analysis in detail of a model analogous to that of PR, incorporating an elementary account of the breakdown process at the tip of a spreading fault. The relevance of the results to fault creep and some related porous media effects are then discussed.

Fracture Mechanics of Shear Faults in Elastic Solids

In this section we cite some results on the fracture mechanics of shear cracks in isotropic elastic solids under plane strain. Principal references to this topic are *Irwin* [1960], *Paris and Sih* [1965], *Rice* [1968], and PR, the last dealing specifically with shear cracks in the way that we shall model them here.

With reference to Figure 1*a*, the stress field near the tip of a freely slipping shear crack loaded so as to induce in-plane deformation of the 'mode II' type has the characteristic singular form

$$\sigma_{ij} \sim K(2\pi r)^{-1/2} f_{ij}(\theta) \qquad \text{as } r \to 0 \tag{1}$$

where $i, j = x, y, z$. The set of functions f_{ij} are independent of loading, and K is a constant referred to as the mode II stress intensity factor. For example,

$$\sigma_{xy} \sim K(2\pi r)^{-1/2} \cos(\theta/2)\,[1 - \sin(\theta/2)\sin(3\theta/2)] \tag{2}$$

For a freely slipping crack the intensity factor is directly proportional to the applied loading. Of greater interest here is the crack with slippage retarded by a frictional stress τ_F acting on the crack faces. In this case the same functional forms as above apply for the near-tip stress singularity, but K is now proportional to the excess of the remotely applied stress over τ_F.

For example, if a freely slipping fault of length l is subject to a remotely applied stress τ_a (see Figure 1*b*), the intensity factor is [*Paris and Sih*, 1965]

$$K = \tau_a(\pi l/2)^{1/2} = 1.25\tau_a l^{1/2} \tag{3}$$

when there is no net entrapped dislocation within the fault (i.e., when the displacement field outside the fault is single-valued, with no net closure failure of the displacement on a surrounding Burgers circuit). When there is a net entrapped dislocation of magnitude just sufficient to annul the stress singularity at one end of the fault, the intensity factor for stresses at the other end is [*Rice*, 1968, equation (318)]

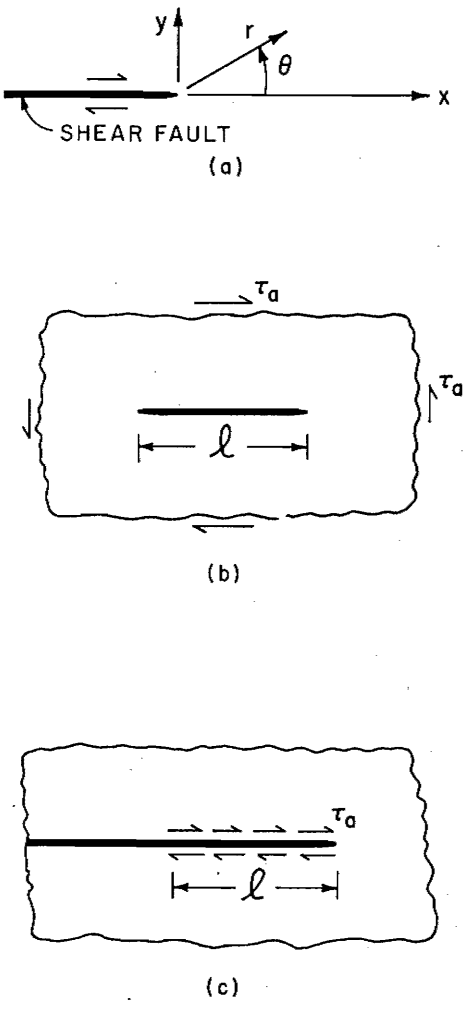

Fig. 1. (*a*) Coordinate systems near tip of a shear fault. (*b*) Finite shear fault. (*c*) Semi-infinite fault, loaded over finite region to simulate finite fault.

$$K = \tau_a(2\pi l)^{1/2} = 2.51\tau_a l^{1/2} \tag{4}$$

To simplify the subsequent mathematics for the case of a porous elastic solid, we will want to consider a semi-infinite fault. This can be employed to simulate a finite fault as follows. We assume that for the purpose of analyzing fault creep, the actual tectonic loading is equivalent to one which, if no slippage were present, would result in a shear stress on the fault plane of magnitude τ_a for a distance l extending back from the tip and of vanishing magnitude over the remainder of the fault (see Figure 1*c*). Such a loading leads to [*Rice*, 1968, equation (98)]

$$K = \tau_a(8l/\pi)^{1/2} = 1.60\tau_a l^{1/2} \tag{5}$$

The numerical factor falls into the range of that for a finite fault with some amount of entrapped dislocation, and we will use the model of Figure 1*c* with the understanding that l can be adjusted so that the crack tip stress intensity corresponds to that of a finite fault.

In all cases for which a retarding frictional stress τ_F acts, the stress intensity factors are as given in these last three equations, but with τ_a replaced by $\tau_a - \tau_F$. For the fault of Figure 1*c*, this means that we consider the stress τ_F to retard motion only over the length l, as is consistent with our interpretation of this model as simulating a finite length fault. Thus with friction, (5) becomes

$$K = (\tau_a - \tau_F)(8l/\pi)^{1/2} = 1.60(\tau_a - \tau_F)l^{1/2} \quad (6)$$

The energy which flows to the crack tip singularity (or, in physical terms, to breakdown processes at the fault tip), per unit of new fault area, is

$$\mathcal{G} = (1 - \nu_e)K^2/(2G) \quad (7)$$

where G is the shear modulus and ν_e is Poisson's ratio. The simplest model of crack advance is the Griffith model, in which no explicit account is taken of processes within the breakdown zone, and a critical value of the driving 'force' $\mathcal{G}$ is assumed to be necessary for fault spreading, where this value is considered characteristic of the material.

On the other hand, an elementary model intended to take some account of breakdown processes at the fault tip has been introduced in PR, as an extension of earlier work associated with the names Barenblatt, Dugdale, and Bilby-Cottrell-Swinden, on cohesive stress models for tensile cracks. The PR model entails the assumption that relative sliding can be initiated when some breakdown stress level τ_B is reached at a point along the prospective fault plane. Once slip is initiated, the resistive shear strength τ is a decreasing function of the amount of a slip δ of one surface of the fault relative to the other; i.e., $\tau = \tau(\delta)$, as illustrated in Figure 2. The function $\tau(\delta)$ approaches the frictional stress τ_F at large δ. *Nason and Weertman* [1973] have suggested that the observed distribution of slip offset would, in fact, require a τ-δ relation of the general shape illustrated.

The PR model is self-contained as regards the prediction of conditions for fault spreading. But in the case of rather brittle behavior, for which the size of the fault tip breakdown zone (defined as the region where $\delta > 0$ and $\tau(\delta) > \tau_F$) is small by comparison to overall length of the slipping region, fault spreading conditions based on the PR model coincide with those based on a critical value of $\mathcal{G}$. Indeed, the connection is that the critical value of $\mathcal{G}$ (or K) is given by

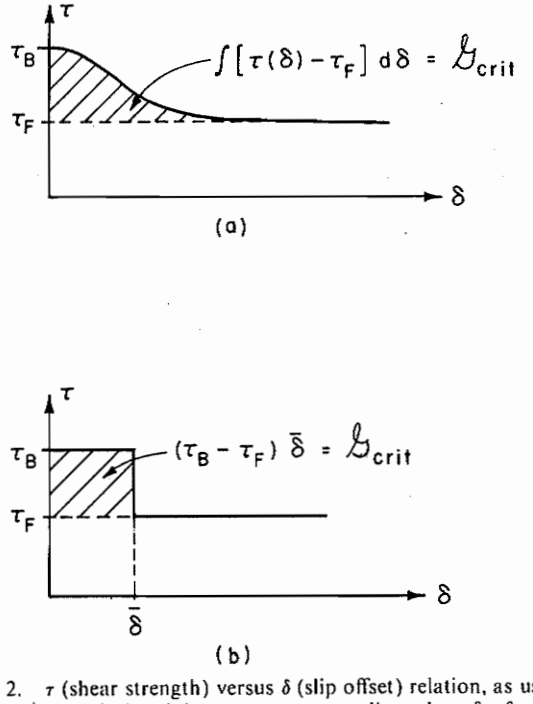

Fig. 2. τ (shear strength) versus δ (slip offset) relation, as used to model processes in breakdown zone at spreading edge of a fault. (*a*) The general case and (*b*) a simplified model. The cross-hatched area can be equated to the fracture energy term, $\mathcal{G}_{crit}$, of fault models that contain no explicit account of the breakdown process.

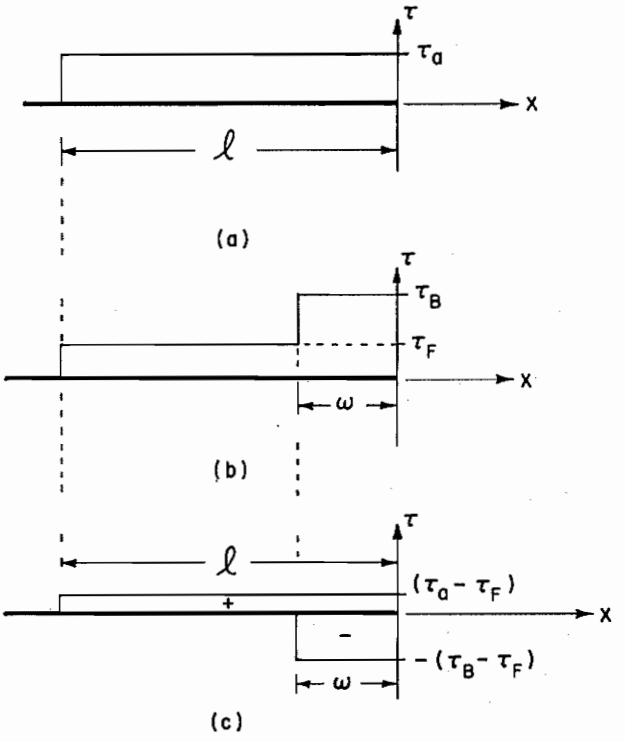

Fig. 3. (*a*) Applied loadings would result in τ_a if no slippage occurred. (*b*) Stress distribution after slippage, in accord with Figure 2*b*. (*c*) Equivalent loadings on freely slipping crack, to compute slippage distribution.

$$\mathcal{G}_{crit} \equiv (1 - \nu_e)K_{crit}^2/(2G) = \int_0^\infty [\tau(\delta) - \tau_F]\, d\delta \quad (8)$$

The integral represents the cross-hatched area in Figure 2. Also, the K which enters the formula is understood to be that for the corresponding fault geometry when solved without explicit account of the breakdown zone, setting $\tau = \tau_F$ along the entire fault surface. These are the same K's as estimated previously, and, for example, by using (6) the critical driving stress corresponding to the fault geometry of Figure 1*c* is then given by

$$\tau_a - \tau_F = \left[\frac{\pi G}{4(1 - \nu_e)l}\int_0^\infty [\tau(\delta) - \tau_F]\, d\delta\right]^{1/2} \quad (9)$$

Since the main parameters of the PR model are τ_B, τ_F, and the cross-hatched area in Figure 2*a*, we may simplify the τ-δ relation as in Figure 2*b* without significant loss of accuracy, where $\bar{\delta}$ is chosen to give the proper cross-hatched area. Then the model can be implemented in a straightforward manner, and we now outline the procedure for the semi-infinite fault model of Figure 1*c*, since this same model is employed subsequently for the porous medium case.

Figure 3*a* shows the stress distribution which, according to the foregoing assumption, applied loads would transmit across the fault plane, were no slippage present. When slip does occur and resistive stresses develop in accord with the τ-δ relation of Figure 2*b*, the stress along the slipped fault varies as shown in Figure 3*b*; τ_B acts in the near-tip region where $\delta < \bar{\delta}$, whereas τ_F acts at greater distances. The slippage that must result in relaxing the stresses from those of Figure 3*a* to those of 3*b* is computed by applying the stress differences shown in Figure 3*c* to a freely slipping crack. Now, neither the magnitude of the applied stress required just to drive the fault, nor the size ω of the breakdown zone is known a priori. These are

determined from the two conditions that (i) there be no net singularity at the fault tip and (ii) the slip δ at distance ω behind the tip be equal to $\bar{\delta}$ of Figure 2*b*.

By successively applying (5) to the positive and negative loadings of Figure 3*c*, we find that the condition of no net singularity is

$$K_{net} = (\tau_a - \tau_F)(8l/\pi)^{1/2} - (\tau_B - \tau_F)(8\omega/\pi)^{1/2} = 0 \qquad (10)$$

Also, by standard methods of crack elasticity analysis [e.g., *Rice*, 1968, equations (22), (70), (87), and (98), implemented as in equations (220)–(223)] the slippage δ is given by

$$\delta = \frac{1 - \nu_e}{G}[(\tau_a - \tau_F)lg(|x|/l) - (\tau_B - \tau_F)\omega g(|x|/\omega)] \qquad (11)$$

where $|x|$ is distance from the fault tip and where the function g is

$$g(\lambda) = \frac{4}{\pi}\left[(\lambda)^{1/2} - \tfrac{1}{2}(1 - \lambda)\log\frac{[1 + (\lambda)^{1/2}]}{|1 - (\lambda)^{1/2}|}\right] \qquad (12)$$

Thus the second condition is obtained by setting $\delta = \bar{\delta}$ in (11) when $|x| = \omega$. The solution can then be expressed parametrically in terms of a variable Q, $0 < Q < 1$, as

$$\tau_a - \tau_F = Q(\tau_B - \tau_F) \qquad \omega = Q^2 l \qquad (13)$$

where Q is given by the lowest root of

$$\frac{\pi G\bar{\delta}}{2(1 - \nu_e)(\tau_B - \tau_F)l} = Q(1 - Q^2)\log\frac{1 + Q}{1 - Q} \qquad (14)$$

or by $Q = 1$ if this equation has no real root.

In practice, our interest is always in the 'brittle' case, corresponding to a small excess of the driving stress τ_a over τ_F and hence to a small ratio ω/l and to $Q \ll 1$. In this case it suffices to retain only the first nonzero term in an expansion of the left side of (14) about $Q = 0$, and we obtain

$$Q = \left[\frac{\pi G\bar{\delta}}{4(1 - \nu_e)(\tau_B - \tau_F)l}\right]^{1/2} \qquad (15)$$

With this value of Q the first of (13) reduces to the prediction of (9), and the size ω of breakdown zone at critical conditions becomes independent of l:

$$\tau_a - \tau_F = \left[\frac{\pi G(\tau_B - \tau_F)\bar{\delta}}{4(1 - \nu_e)l}\right]^{1/2} \qquad \omega = \frac{\pi G\bar{\delta}}{4(1 - \nu_e)(\tau_B - \tau_F)} \qquad (16)$$

Some insight into porous media effects on fault propagation may be obtained simply by observing that the critical conditions (16) depend on ν_e, which will be equated either to ν_u or ν in the respective limits of completely undrained and completely drained response. Since $\nu_u > \nu$, this observation in itself implies a certain degree of stabilization with increasing fault spreading speed, as noted in RC. But we may now surmise, and indeed will demonstrate in what follows, that the effect is even greater, in that the greatest resistance to spreading occurs when the deformation is undrained on the scale of overall fault length l but drained locally on the smaller size scale of the breakdown zone ω.

All considerations here are for 'in-plane' (or mode II) fault motion. However, formulae identical to (3)–(16) result for antiplane (mode III) fault motion, except that ν_e should everywhere be replaced by zero. This implies that there is no corresponding porous media effect on antiplane fault motion. General three-dimensional faults involve, at different locations along their periphery, both in-plane and antiplane motions, and thus it is the in-plane segments which should be most stabilized through the mechanism discussed here.

Plane Strain Equations for Porous Elastic Media

We follow the presentation in RC of the linear Biot constitutive relations for isotropic, fluid-infiltrated, porous elastic solids, with compressible constituents. These differ from the equations given by *Biot* [1941] only in that the material constants introduced by Biot have been replaced by different parameters that are more readily open to physical interpretation. The relations are (in indicial notation, $i, j = x, y, z$, with summation convention)

$$\epsilon_{ij} = (2G)^{-1}\{\sigma_{ij} - [\nu/(1 + \nu)]\delta_{ij}\sigma_{kk} + [3(\nu_u - \nu)/B(1 + \nu)(1 + \nu_u)]\delta_{ij}p\} \qquad (17a)$$

$$m - m_0 = [3\rho_0(\nu_u - \nu)/2GB(1 + \nu)(1 + \nu_u)]\cdot[\sigma_{kk} + (3/B)p] \qquad (17b)$$

$$q_i = -\rho_0\kappa\partial p/\partial x_i \qquad (17c)$$

Equations (17*a*) and (17*b*) relate the total stress (σ_{ij}) and pore pressure (p) to the strain (ϵ_{ij}) and fluid mass (m) per unit volume of the medium. In these, G is the elastic shear modulus (this modulus is the same under either drained (p = const) or undrained (m = const) conditions), ν is the Poisson's ratio under drained conditions, and ν_u is the ratio under undrained conditions. We note that ν_u satisfies $\nu < \nu_u < \frac{1}{2}$, the lower limit being approached for a highly compressible pore fluid, and the upper limit when both the solid and the fluid constituents, taken separately, are much less compressible than the drained porous medium. The constant B is defined so that $p = -B\sigma_{kk}/3$ is the pressure induced when stress is applied under undrained conditions. Also, $0 < B < 1$, the upper and lower limits being approached under the same conditions as those for ν_u. The fluid mass content in the unstressed state is m_0, and ρ_0 is the corresponding mass density of the pore fluid. Equation (17*c*) is Darcy's law, where q_i is the mass flux rate per unit area and κ is the permeability. The latter is sometimes written $\kappa = k/\mu$, where k has units of length squared and μ is the viscosity of the pore fluid. The relation of the new parameters B and ν_u to those of Biot is discussed in RC, where numerical values of B and ν_u are also tabulated for some porous rocks. Of course, for fully saturated clay soils we may take $B = 1$ and $\nu_u = \frac{1}{2}$.

The full set of field equations is obtained by appending to the constitutive relations (17*a*)–(17*c*) equations based on the relevant physical principles of (i) stress field equilibrium, (ii) strain compatibility, and (iii) mass conservation for the diffusing pore fluid. In RC these equations are expressed in terms of stress and pore pressure as basic variables; for the case of plane strain (say, in the x-y plane) they become as follows: (i) equilibrium,

$$\partial\sigma_{xx}/\partial x + \partial\sigma_{xy}/\partial y = 0 \qquad \partial\sigma_{xy}/\partial x + \partial\sigma_{yy}/\partial y = 0 \qquad (18)$$

(ii) strain compatibility, in combination with (i),

$$\nabla^2(\sigma_{xx} + \sigma_{yy} + 2\eta p) = 0 \qquad (19)$$

where $\eta = 3(\nu_u - \nu)/2B(1 + \nu_u)(1 - \nu)$ and (iii) mass conservation, in combination with (i) and (ii),

$$(c\nabla^2 - \partial/\partial t)[\sigma_{xx} + \sigma_{yy} + (2\eta/\mu)p] = 0 \qquad (20)$$

where $\mu = (\nu_u - \nu)/(1 - \nu)$ and where

$$c = [2G\kappa(1 - \nu)/(1 - 2\nu)] \cdot [B^2(1 + \nu_u)^2(1 - 2\nu)/9(1 - \nu_u)(\nu_u - \nu)]$$

Here t is time and $\nabla^2 = \partial^2/\partial x^2 + \partial^2/\partial y^2$. We note also that the alteration in fluid mass content, $m - m_0$, is proportional to the bracketed term appearing in (20) and hence satisfies the diffusion equation.

Formulation for Steadily Advancing Shear Fault

Here, using the field equations (18)–(20), we formulate the coupled deformation-diffusion problem of a steadily advancing shear fault in a porous elastic medium. To reduce the mathematics to a tractable level, we consider only the semi-infinite fault in an infinite body, as shown in Figure 1*c*, and assume that points of load application move at the same speed as that of the fault tip, so that a steady deformation field results. Specifically, if f is any field variable, we assume that its dependence on x, y, and t has the form

$$f = f(x - Vt, y) \qquad (21)$$

where V is the speed at which the fault advances in the direction of the x axis. Thus we may examine the field at any particular time t, and we choose that for which the origin of the x, y system coincides with the fault tip as in Figure 1*a*. Also, the last of the field equations (18)–(20) may be rewritten as

$$(c\nabla^2 + V\,\partial/\partial x)[\sigma_{xx} + \sigma_{yy} + (2\eta/\mu)p] = 0 \qquad (22)$$

and the problem can be formulated with only x and y regarded as independent variables.

The problem is antisymmetric about the x axis, so that the stresses and pore pressure satisfy

$$\sigma_{xx}(x, y) = -\sigma_{xx}(x, -y) \qquad \sigma_{xy}(x, y) = \sigma_{xy}(x, -y)$$
$$\sigma_{yy}(x, y) = -\sigma_{yy}(x, -y) \qquad p(x, y) = -p(x, -y) \qquad (23)$$

Hence the problem can be formulated in the upper half plane $y \geq 0$, $-\infty < x < \infty$.

The antisymmetry requirements give boundary conditions

$$\sigma_{xx}(x, 0) = \sigma_{yy}(x, 0) = p(x, 0) = 0 \qquad 0 < x < \infty \qquad (24)$$

Similarly, since σ_{yy} and p must be continuous across the fault line,

$$\sigma_{yy}(x, 0) = p(x, 0) = 0 \qquad -\infty < x < 0 \qquad (25)$$

The final boundary condition on the fault is given by prescribing the shear loading there as some function $\tau(x)$:

$$\sigma_{xy}(x, 0) = -\tau(x) \qquad -\infty < x < 0 \qquad (26)$$

The minus sign occurs to preserve the sort of sign convention adopted in Figure 1*c* and Figure 3*c* for shear loading. Finally, it is required that all the σ's and p vanish as $|x| \to \infty$, $y \to \infty$.

The solution to the governing differential equations (18), (19), and (22) subject to the above boundary conditions is developed, through Fourier transform and Wiener-Hopf techniques in the appendix, for the special shear loading function

$$\tau(x) = \tau^{(\lambda)}(x) \equiv e^{i\lambda x} \qquad (27)$$

As suggested already by the notation in (27), fields corresponding to this loading will be denoted generically by $f^{(\lambda)}(x, y)$. Although such fields have little intrinsic interest, fields $f(x, y)$ corresponding to an arbitrary loading $\tau(x)$ may be written in terms of $f^{(\lambda)}(x, y)$ by Fourier superposition in a manner to be discussed presently.

The constants $A^{(\lambda)}(\kappa)$, $B^{(\lambda)}(\kappa)$, and $C^{(\lambda)}(\kappa)$, given by (A10) in the appendix, may be employed along with (A6*b*) and the inversion formula (A1*b*) to write

$$\sigma_{xy}^{(\lambda)} = -(1/2\pi)\int_{-\infty}^{+\infty} \{[i\kappa C^{(\lambda)}(\kappa)/m(\kappa) + i\kappa y A^{(\lambda)}(\kappa)] \cdot \exp[-m(\kappa)y] + 2n(\kappa)(c/V)B^{(\lambda)}(\kappa) \cdot \exp[-n(\kappa)y]\} \exp(i\kappa x)\, d\kappa \qquad (28)$$

The integral cannot be evaluated in closed form everywhere. However, by replacing x, y by polar coordinates r, θ (see Figure 1*a*) and performing an asymptotic analysis for $r \to 0$, a lengthy but straightforward calculation leads to the remarkable result

$$\sigma_{xy}^{(\lambda)} \sim K^{(\lambda)}(2\pi r)^{-1/2} \cos(\theta/2)[1 - \sin(\theta/2)\sin(3\theta/2)] \qquad (29)$$

where

$$K^{(\lambda)} = (2)^{1/2} \exp(-i\pi/4)/[D^-(\lambda)m^-(\lambda)] \qquad (30)$$

and the functions $D^-(\lambda)$, $m^-(\lambda)$ are given by (A3), (A13), (A14), and (A16) in the appendix.

This fault tip singularity in $\sigma_{xy}^{(\lambda)}$ is of the same r, θ dependence as that for cracks in elastic solids (see (2)). The other stresses $\sigma_{xx}^{(\lambda)}$, $\sigma_{yy}^{(\lambda)}$ could likewise be shown to have the same singular form as that in elastic solids, whereas the pore pressure $p^{(\lambda)}$ is found to be bounded in the neighborhood of the crack tip and to vanish at the tip itself. Thus near the crack tip the pressure term in the stress-pressure-strain relation (17*a*) is insignificant compared to the stress terms, near-tip displacements computed by integration of these strains will be indistinguishable from those of an elastic body with properties corresponding to those of drained response, i.e., $\nu_e = \nu$, and we say that the material always responds in a drained fashion immediately at the crack tip. This is notwithstanding the fact that for sufficiently rapid fault propagation, material elements at any fixed distance away from the tip will respond in an effectively undrained manner.

By the Fourier inversion formula (A1*b*), any arbitrary fault shear loading function $\tau(x)$ may be written in the form

$$\tau(x) = \frac{1}{2\pi}\int_{-\infty}^{\infty} \bar{\tau}(\lambda)e^{i\lambda x}\, d\lambda \qquad (31)$$

where $\bar{\tau}(\lambda)$ is given by (A9*a*). Thus by the principle of superposition, any field quantity $f(x, y)$ corresponding to the loading $\tau(x)$ may be expressed in terms of $f^{(\lambda)}(x, y)$ by

$$f(x, y) = \frac{1}{2\pi}\int_{-\infty}^{\infty} f^{(\lambda)}(x, y)\bar{\tau}(\lambda)\, d\lambda \qquad (32)$$

This formalism extends to the stress intensity factor K, i.e.,

$$K = \frac{1}{2\pi}\int_{-\infty}^{\infty} K^{(\lambda)}\bar{\tau}(\lambda)\, d\lambda \qquad (33)$$

Uniform Shear Loading on Steadily Advancing Fault

We now consider specifically the case of uniform shear loading over a distance l on a frictional fault, i.e.,

$$\tau(x) = \tau_a - \tau_F \qquad -l < x < 0$$
$$\tau(x) = 0 \qquad x < -l \tag{34}$$

(see Figure 1c). The corresponding $\tilde{\tau}$ is given by (A9a) as

$$\tilde{\tau}(\lambda) = -(\tau_a - \tau_F)[1 - \exp(i\lambda l)]/(i\lambda) \tag{35}$$

From (30), (33), and (35) we obtain a stress intensity factor

$$K = \frac{-1}{i\pi(2)^{1/2}}(\tau_a - \tau_F)e^{-i\pi/4} \cdot \int_{-\infty}^{+\infty} \{[1 - e^{i\lambda l}]/[\lambda D^-(\lambda)m^-(\lambda)]\}\, d\lambda \tag{36}$$

By letting $s = \lambda l$, this may be rewritten in the form

$$K = (\tau_a - \tau_F)(8l/\pi)^{1/2}h(Vl/c) = K_{\text{nom}}h(Vl/c) \tag{37}$$

where the nominal stress intensity factor K_{nom} is that given by (6) and the dimensionless function h of the dimensionless speed measure Vl/c is given by

$$h(\gamma) = \frac{-e^{-i\pi/4}}{4i\pi^{1/2}} \int_{-\infty}^{+\infty} \frac{1 - e^{is}}{s\hat{D}^-(s,\gamma)\hat{m}^-(s)}\, ds \tag{38}$$

with

$$\hat{D}^-(s,\gamma) = \beta + [2is(\beta - 1)/\gamma][1 - \hat{n}^-(s,\gamma)/\hat{m}^-(s)]$$
$$\hat{n}^-(s,\gamma) = (s - i\gamma)^{1/2} \qquad \hat{m}^-(s) = s^{1/2} \tag{39}$$

The new quantity β (>1) is defined by

$$\beta \equiv 1/(1 - \mu) = (1 - \nu)/(1 - \nu_u) \tag{40}$$

and we shall see later that β plays an important role as a measure of the maximum possible increase that the porous media effects under consideration can cause in forcing parameters for fault spreading. Also, in accord with the similar functions in the appendix, $\hat{n}^-$ and $\hat{m}^-$ have their branch cuts on the positive imaginary axis of the complex s plane and are such that both have positive real parts when $s > 0$.

The function $h(\gamma)$ is most readily evaluated after shifting the integration contour to one which wraps around the branch cut in the upper half s plane, yielding

$$h(\gamma) = \frac{1}{2\pi^{1/2}} \int_0^\infty \frac{1 - e^{-\eta}}{\eta^{3/2}} \operatorname{Re}\left[\frac{1}{\hat{D}_r^-(i\eta,\gamma)}\right] d\eta \tag{41}$$

where $\hat{D}_r^-(i\eta,\gamma)$ is the limit of $\hat{D}^-(s,\gamma)$ as s approaches a point $i\eta$ on the positive imaginary s axis from the right. When $Vl/c \to 0$, $h(Vl/c) \to 1$ and (37) reduces to (6) for the elastic solid. This is as it should be, since the response is completely drained in this limit and the material behaves as though elastic with parameters G and ν. As Vl/c increases from zero to infinity, $h(Vl/c)$ decreases monotonically from 1 to $1/\beta$. Hence it is seen that the stress intensity factor is reduced continuously with spreading speed, the maximum possible reduction being by the factor $1/\beta$. This seems at first somewhat paradoxical, for one would expect response as an elastic solid with parameters G and ν_u as $Vl/c \to \infty$ and thus would expect (6) likewise to be valid in this limit. The explanation is simple, however, and will be explored more fully in subsequent sections. The crux of the explanation is that, as was noted in the previous section, for any finite speed V there is always an effectively drained region immediately at the crack tip, with stress singularity governed by the K computed here. But this drained kernel at the crack tip has a size only of the order of the characteristic diffusion length c/V. At greater distances the behavior is effectively undrained, and as $V \to \infty$ the size of the drained kernel shrinks to zero, and the elastic solution for an undrained material is recovered outside it.

This discussion also reveals the physical reason for the reduction of K with speed. Very approximately, we may think of the material as an elastic solid of undrained properties containing a softer elastic inclusion, of drained properties, in the drained kernel regions at the fault tip and along the fault surfaces. Since deformations are effectively imposed on the softer near-tip region by the stiffer outer region, the near-tip stresses are smaller than would result if the entire body were composed of the stiff material.

Indeed, the actual factor $1/\beta$ that results for the reduction as $Vl/c \to \infty$ can be rationalized in this way, since near-tip displacements along the fault surface should be proportional to $(1 - \nu)K/G$ if computed from the elastic field in the drained kernel and to $(1 - \nu_u)K_{\text{nom}}/G$ if computed from the elastic field outside. By equating these two expressions we obtain

$$K = [(1 - \nu_u)/(1 - \nu)]K_{\text{nom}} = (1/\beta)K_{\text{nom}} \tag{42}$$

as $Vl/c \to \infty$, in accord with our detailed calculation.

Fault-Spreading Criterion Based on Critical Energy Release Rate

Before further developing the solution for uniform shear loading and applying it to a detailed model of fault spreading, we shall first examine the simpler model of the Griffith type, in which a critical energy release rate is postulated, but no specific account is taken of processes within the breakdown zone at the fault tip. Since the crack tip singularity, which is the source of the energy flux, corresponds to drained behavior, we use the drained elastic properties in (7) for $\mathcal{G}$, with (37) for K, to obtain

$$\mathcal{G} = (1 - \nu)K^2/(2G) = \mathcal{G}_{\text{nom}}h^2(Vl/c) \tag{43}$$

where the nominal energy release rate, phrased in terms of drained properties, is

$$\mathcal{G}_{\text{nom}} \equiv (1 - \nu)K_{\text{nom}}^2/(2G) = 4(1 - \nu)(\tau_a - \tau_F)^2 l/(\pi G) \tag{44}$$

Thus if a critical energy release rate $\mathcal{G}_{\text{crit}}$ is required for fault advance (where $\mathcal{G}_{\text{crit}}$ could be related to parameters of a more elaborate fracture model as in (8), i.e., as the cross-hatched area in Figure 2), then the criterion for fault spreading at speed V is

$$\mathcal{G}_{\text{nom}} = \mathcal{G}_{\text{crit}}/[h^2(Vl/c)] \tag{45}$$

This relation is plotted in Figure 4 for various values of β [$=(1 - \nu)/(1 - \nu_u)$], where the function h has been computed numerically from (41). For example, the curve corresponding to $\beta = 1.33$ would result if $\nu = 0.2$ and $\nu_u = 0.4$, which we consider to be reasonable values for a fissured rock mass. Higher values of β result for parameters descriptive of overconsolidated clay soils; e.g., $\beta = 1.7$ if $\nu = 0.15$ and $\nu_u = 0.5$.

Since $h \to 1/\beta$ for large Vl/c, we see that $\mathcal{G}_{\text{nom}}$ increases from $\mathcal{G}_{\text{crit}}$ at low speeds to a maximum of

$$(\mathcal{G}_{\text{nom}})_{\max} = \beta^2\mathcal{G}_{\text{crit}} \tag{46}$$

at rapid spreading speeds. This is a numerically significant effect, and we shall discuss it later in relation to observations on fault creep.

Physically, however, there are two restrictions on the validity of the criterion based on a critical energy release rate. First,

as was discussed already in connection with the elastic case, it is necessary that the breakdown zone be small in comparison to overall fault length. In the present context it is also necessary that the drained kernel at the fault tip be sufficiently large to envelop fully the breakdown zone. This latter requirement cannot be met at high spreading speeds, since the kernel size is proportional to c/V.

Indeed, if in the high-speed limit we simply assume elastic response with undrained material properties and postulate the same critical value of $\mathcal{G}$, we would predict (see RC)

$$\mathcal{G} = (1 - \nu_u)K_{\text{nom}}^2/(2G) = \mathcal{G}_{\text{crit}} \tag{47}$$

or, since we have defined $\mathcal{G}_{\text{nom}}$ in terms of drained properties,

$$\mathcal{G}_{\text{nom}} \equiv (1 - \nu)K_{\text{nom}}^2/(2G) = [(1 - \nu)/(1 - \nu_u)]\mathcal{G}_{\text{crit}} = \beta\mathcal{G}_{\text{crit}} \tag{48}$$

The more elaborate fracture model considered next shows that this is indeed a proper limit as $Vl/c \to \infty$. However, we are more interested instead in the maximum value of the driving force which, according to the more elaborate model, occurs at some intermediate value of Vl/c and is closer to the factor β^2 of (46) than to the factor β of (48), at least when the breakdown zone size is small.

Fault-Spreading Criterion Based on τ-δ Relation for Breakdown Zone

We now consider an extension of the PR model to the case of a porous elastic medium. The τ-δ relation is taken as the simplified one of Figure 2*b*, so the stress redistribution along the advancing fault is as shown in Figure 3*c*. But this is just a superposition of two uniform shear loadings, each of the type analyzed in detail in the foregoing. In order to determine the unknowns in the problem (say, ω and $\tau_a - \tau_F$) we require, analogously to (10), that (i) there be no net stress singularity at the fault tip and (ii) the slip offset at the trailing edge of the breakdown zone be equal to $\bar{\delta}$.

By (37), then, the first condition becomes

$$K_{\text{net}} = (\tau_a - \tau_F)(8l/\pi)^{1/2}h(Vl/c) - (\tau_B - \tau_F)(8\omega/\pi)^{1/2}h(V\omega/c) = 0 \tag{49}$$

Now in order to enforce the second condition we must develop an expression for sliding displacements along the fault. A formula is developed in the appendix, (A22), for the sliding displacement $\delta^{(\lambda)}(x)$ corresponding to the shear loading $\tau^{(\lambda)}(x)$. First we superpose this for the single uniform shear loading of (34), for which $\bar{\tau}(\lambda)$ is given by (35). By the superposition formalism of (32) the slip offset induced by this loading is

$$\delta(x) = \frac{1}{2\pi}\int_{-\infty}^{+\infty} \bar{\tau}(\lambda)\delta^{(\lambda)}(x)\, d\lambda = [(1 - \nu)(\tau_a - \tau_F)l/G]g(|x|/l,\ Vl/c) \qquad x < 0 \tag{50}$$

where, upon writing $s = \lambda l$ and using the same notation as in (38) and (39), the function g is given by

$$g(\alpha, \gamma) = \frac{-1}{i\pi}\int_{-\infty}^{+\infty} \frac{(1 - e^{is})e^{-is\alpha}\ \text{erf}\,[e^{-i\pi/4}\hat{m}^-(s)\alpha^{1/2}]}{s^2\hat{D}^-(s, \gamma)}\, ds \tag{51}$$

A simpler representation, applicable for $0 \le \alpha \le 1$ and more amenable to numerical evaluation, can be obtained by adding and subtracting a term proportional to $\hat{m}^-(s)$ to the numerator of the integrand. In this way the integral can be rewritten as

$$g(\alpha, \gamma) = \frac{1}{i\pi}\int_{-\infty}^{+\infty} \frac{e^{i(1-\alpha)s}\ \text{erf}\,[e^{-i\pi/4}\hat{m}^-\alpha^{1/2}] - 2\pi^{-1/2}e^{-i\pi/4}\hat{m}^-\alpha^{1/2}}{s^2\hat{D}^-}\, ds + \frac{1}{i\pi}\int_{-\infty}^{+\infty} \frac{2\pi^{-1/2}e^{-i\pi/4}\hat{m}^-\alpha^{1/2} - e^{-is\alpha}\ \text{erf}\,[e^{-i\pi/4}\hat{m}^-\alpha^{1/2}]}{s^2\hat{D}^-}\, ds \tag{52}$$

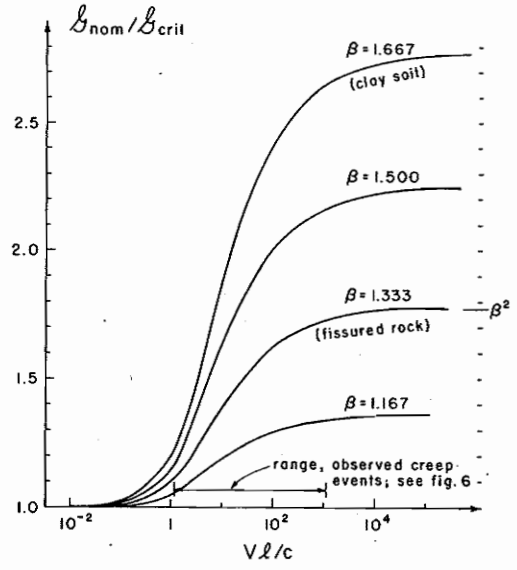

Fig. 4. A plot of the fault spreading criterion $\mathcal{G}_{\text{nom}} = \mathcal{G}_{\text{crit}}/h^2(Vl/c)$, based on a critical energy release rate, for various values of β, where $\beta = (1 - \nu)/(1 - \nu_u)$.

The second integrand is analytic everywhere in the lower half of the s plane. Since the integral can be closed without contribution by a contour at ∞, the integral itself must vanish by the Cauchy integral formula. Only the first integral remains, and by distorting its path to lie along the branch cut on the positive imaginary s axis and setting $s = i\eta$, we obtain

$$g(\alpha, \gamma) = \frac{2}{\pi}\int_0^{\infty} \{2(\alpha\eta/\pi)^{1/2} - e^{-(1-\alpha)\eta} \cdot \text{erf}\,[(\alpha\eta)^{1/2}]\}\ \text{Re}\left[\frac{1}{\eta^2\hat{D}_r^-(i\eta, \gamma)}\right] d\eta \tag{53}$$

We now return to the fracture model and compute the total slip offset by superposing the response to the two uniform shear loadings shown in Figure 3*c*. Thus using (50) analogously to (11) for the elastic case, we have

$$\delta = \frac{1 - \nu}{G}\left[(\tau_a - \tau_F)lg\left(\frac{|x|}{l}, \frac{Vl}{c}\right) - (\tau_B - \tau_F)\omega g\left(\frac{|x|}{\omega}, \frac{V\omega}{c}\right)\right] \tag{54}$$

By setting $\delta = \bar{\delta}$ when $|x| = \omega$ in this equation, we obtain an

equation which, together with (49), may be solved (in principle) for the unknowns ω and $\tau_a - \tau_F$.

In this manner the required driving stress for any given fault speed V is expressed parametrically, in terms of the unknown ω, by

$$\tau_a - \tau_F = (\tau_B - \tau_F)(\omega/l)^{1/2}h(V\omega/c)/h(Vl/c) \qquad (55)$$

where ω is determined from

$$\frac{G\bar{\delta}}{(1-\nu)(\tau_B - \tau_F)l} = (\omega/l)^{1/2}h(V\omega/c) \cdot g(\omega/l,\ Vl/c)/h(Vl/c) - (\omega/l)g(1,\ V\omega/c) \qquad (56)$$

In Figure 5 we have plotted the left-hand side of (56) as a function of Vl/c for some values of ω/l. The results shown are for $\beta = 1.33$. We conclude that for a given $\bar{\delta}$, the corresponding size ω of the breakdown zone varies only slightly as the fault velocity V varies over several orders of magnitude. Thus since the numerical calculations involved in solving (56) are very costly, we plot in Figure 6 the dimensionless driving stress $\mathcal{G}_{nom}/\mathcal{G}_{crit}$ as a function of Vl/c for fixed ω/l, rather than for fixed $G\bar{\delta}/[(1-\nu)(\tau_B - \tau_F)l]$, as would appear to be more natural. Indeed, defining $\mathcal{G}_{crit}$ as $(\tau_B - \tau_F)\bar{\delta}$, we obtain, by taking the ratio of the square of (55) to (56),

$$\mathcal{G}_{nom}/\mathcal{G}_{crit} \equiv 4(1-\nu)(\tau_a - \tau_F)^2 l/[\pi G(\tau_B - \tau_F)\bar{\delta}] = \frac{4h^2(V\omega/c)}{\pi h(Vl/c)[(l/\omega)^{1/2}h(V\omega/c)g(\omega/l,\ Vl/c) - h(Vl/c)g(1,\ V\omega/c)]} \qquad (57)$$

The curves in Figure 6 show this equation for $\omega/l = 10^{-4}$, 10^{-3}, 10^{-2}, and 10^{-1}. Also shown is a curve marked $\omega/l = 0$, which is the same curve as plotted in Figure 4 for $\beta = 1.33$. We see that the expected undrained limit β is now approached as $V \to \infty$, when the finite size ω of the breakdown zone, by comparison to c/V, is taken into account. It must be assumed, however, that at speeds greater than that at which the maximum occurs, the fault will become unstable, since $\mathcal{G}_{nom}$ versus V is then decreasing.

Specifically, the viewpoint toward seismic instability that arises from this model is that a fault is stable at slow speeds and at speeds up to the peak in the curve, since in this range an increasing value of driving force is necessary to obtain increasing speed. But at a critical driving force, corresponding to the peak, no quasi-static solution for fault spreading exists in response to a further increment in driving force, and unstable dynamic fault motion ensues.

Since our interest is primarily in cases for which $\omega/l \ll 1$, it is possible to make use of the result

$$g(\alpha, \gamma)/\alpha^{1/2} \to (8/\pi)h(\gamma) \qquad \text{as} \qquad \alpha \to 0 \qquad (58)$$

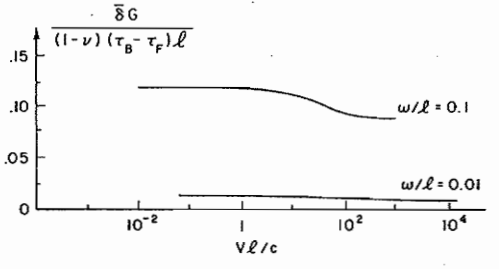

Fig. 5. Variation of $\bar{\delta}$ with fault-spreading speed for constant values of ω. Calculations are for $\beta = 1.33$.

derived from (41) and (53), and thus to write

$$\mathcal{G}_{nom}/\mathcal{G}_{crit} = \frac{h^2(V\omega/c)}{[2h(V\omega/c) - (\pi/4)g(1,\ V\omega/c)]}\frac{1}{h^2(Vl/c)} \qquad (59)$$

We note further that

$$(\pi/4)g(1, 0) = 1 \qquad (\pi/4)g(1, \infty) = 1/\beta \qquad (60)$$

so that $(\pi/4)g(1, \gamma)$ has the same limiting values as $h(\gamma)$. It is now easy to check the following special cases:

In case 1, where $V\omega/c \to 0$, $Vl/c \to 0$ (with ω/l fixed), there is completely drained behavior, in which case

$$\mathcal{G}_{nom} = \mathcal{G}_{crit} \qquad (61)$$

In case 2, where $V\omega/c \to 0$ and Vl/c is fixed, there is drained behavior over the size scale of the breakdown zone but not necessarily overall, in which case

$$\mathcal{G}_{nom} = [1/h^2(Vl/c)]\mathcal{G}_{crit} \qquad (62)$$

This agrees with the criterion of a critical energy release rate, based on the singularity within the drained fault-tip kernel; the $\mathcal{G}_{nom}$ versus V curve is monotonically rising.

In case 3, where $V\omega/c$ is fixed and $Vl/c \to \infty$, there is undrained behavior on the overall size scale but not necessarily over that of the breakdown zone, in which case

$$\mathcal{G}_{nom} = \{h^2(V\omega/c)/[2h(V\omega/c) - (\pi/4)g(1,\ V\omega/c)]\}\mathcal{G}_{crit} \qquad (63)$$

and the $\mathcal{G}_{nom}$ versus V curve is unstably falling.

In case 4, where $V\omega/c \to \infty$ and $Vl/c \to \infty$ (with ω/l fixed), there is completely undrained behavior, in which case

$$\mathcal{G}_{nom} = \beta\mathcal{G}_{crit} \qquad (64)$$

the expected result, since we have defined $\mathcal{G}_{nom}$ on the basis of the drained Poisson's ratio.

We note further that if ω/l is sufficiently small, there must be a value of V for which the limits $V\omega/c \to 0$, $Vl/c \to \infty$ are effectively attained, in which case there results the maximum possible value,

$$\mathcal{G}_{nom} = \beta^2\mathcal{G}_{crit} \qquad (65)$$

However, we see from the plots in Figure 6 that ω/l must be very small indeed for the actual maximum to coincide closely with the factor β^2.

Numerical Data Based on Creep Events on the San Andreas Fault System in Central California

As shown in Figures 4 and 6, our mathematical solution predicts the requirement of an increasing driving force to increase the speed at which a shear fault spreads quasi-statically. The effect is numerically significant, and it is due to the coupling of deformation and fluid diffusion in the surrounding rock.

Provided that the speeds and lengths of observed creep

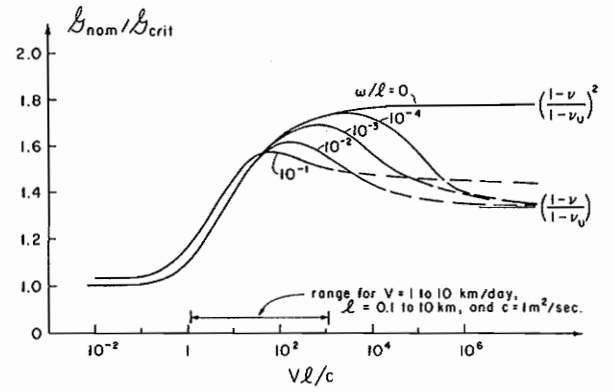

Fig. 6. The nominal energy release required for fault spreading, as a function of fault velocity, based on the τ-δ relation of Figure 2*b*. The curves are drawn for $(1 - \nu)/(1 - \nu_u) = 1.333$, and results for different ratios, ω/l, of breakdown zone size to fault length are shown. The range of Vl/c corresponding to observed fault creep events [*King et al.*, 1973; *Nason and Weertman*, 1973] on the San Andreas system in central California is also shown, when a value of c suggested by *Anderson and Whitcomb* [1975] is used.

events correspond to those portions of the Vl/c axis over which $\mathcal{G}_{nom}$ is steeply rising, it can be assumed that the observed faults are being stabilized against rapid spreading by the effect that we have described and hence that this effect could be the physical mechanism which makes fault creep (versus unstable, seismic slippage) possible. Using data on creep events on the San Andreas fault system in central California, as reported by *King et al.* [1973] and by *Nason and Weertman* [1973], we find that observations do indeed lend credence to the above statement.

Representative speeds of creep events are reported by these sources to lie in the range of 1–10 km/d, with some occasionally faster, and slip lengths l lie in the range of 0.1–10 km. The diffusivity c in the San Andreas region is not accurately known, but *Anderson and Whitcomb* [1975] suggest that a field value of approximately 1 m²/s is consistent with a number of indirect observations. The value is much higher than what one would normally associate with diffusion phenomena and is certainly higher than that for water motion in, say, clay soils or competent rocks (excepting porous sandstones, which can have c values in this range; see RC). However, the value is consistent with a permeability κ which does not seem at all high for fissured or jointed rock masses in or near to a fault zone. This we compute from the last of (20), setting $c = 1$ m²/s and choosing $G = 2 \times 10^4$ MN/m² (=2×10^5 bars), $\nu = 0.2$, $\nu_u = 0.4$, and $B = 0.6$. The result is $\kappa \approx 5 \times 10^{-5}$ m⁴/MN s, which corresponds to about 50 millidarcys but is perhaps better appreciated when reported as the flow rate of pore water that would be induced by a pressure gradient of 10^{-2} MN/m³ (or 1 bar/10 m, a magnitude for which the drop in pore pressure over some length Δx is equal to the pressure at the base of a vertical column of the same length at the earth's surface). This flow rate is 5×10^{-4} kg/m² s, and the corresponding average velocity of the water flowing in fissures or joints would range from about 0.5 to 0.05 mm/s if these occupied a volume fraction ranging from 0.1% to 1%. These numbers do not seem unreasonable for fissured rock near a fault zone, and thus we accept the indirectly inferred value of Anderson and Whitcomb, $c = 1$ m²/s. Certainly, for actual faults the spatial nonuniformity of elastic and fluid transport properties will affect the conditions of drainage near the fault tip; high permeability near the tip could allow drained conditions at speeds beyond what is predicted based on a 'representative' value of c, as above.

Using this value of c and the range of speeds and slip lengths reported above, we can find the corresponding range of values of the dimensionless speed parameter Vl/c for the observed creep events. This range is marked on Figure 6 and also on Figure 4. The results are highly encouraging, in that this range corresponds nicely to that part of the Vl/c axis over which the required fault driving force, $\mathcal{G}_{nom}$, is steeply increasing. Thus while there may be several other effects that contribute to fault creep (as outlined in the introduction), it does indeed seem highly probable, on the basis of this observation alone, that the fluid interaction effect described here was active in providing significant stabilization to those faults on which the creep measurements have been taken.

A more detailed comparison of creep data with the predictions of our model requires choice of the breakdown zone size ω. This is unknown, but we shall suggest subsequently, based in part on a constraint provided by some observations of *King et al.* [1973], that a reasonable value for ω is of the order of 1 m or smaller. Hence, given the range of slip lengths cited above, namely, 0.1–10 km, ω/l should always be very small, lying in the range from 10^{-2} to 10^{-4} or smaller values.

Consider, then, a fault with slip length $l = 1$ km, so that $\omega/l = 10^{-3}$ or less, and assume that the β value on which Figure 6 is based (consistent with $\nu = 0.2$, $\nu_u = 0.4$) adequately describes rock near the fault. Estimating c as before, we find that propagation speeds of $V = 1$ and 10 km/d correspond to values of 11.6 and 116, respectively, for Vl/c. The associated values of the required fault driving force, in the form $\mathcal{G}_{nom}/\mathcal{G}_{crit}$, are 1.41 and 1.63, respectively. For comparison, the minimum value of $\mathcal{G}_{nom}/\mathcal{G}_{crit}$ to move a fault is 1, and the value corresponding to the peak in the curve, beyond which it is assumed that seismic propagation must ensue, is 1.69 for $\omega/l = 10^{-3}$ or 1.74 for $\omega/l = 10^{-4}$.

Now consider the maximum possible speeds of fault creep, corresponding to the maxima in the curves of Figure 6. If we take $\omega = 1$ m, then we find $V_{max} = 154$ km/d for $l = 0.1$ km, 54 km/d for $l = 1$ km, and 22 km/d for $l = 10$ km. The values would be larger for a smaller value of ω. For comparison, the largest values reported by King, Nason, and Tocher are 80 km/d for an event in which the rupture length was not recorded and 24 km/d initially for an event which spread, at decreasing speed, over approximately 6 km.

Our estimate of $\mathcal{G}_{crit}$ and thus, approximately, of ω is based on this latter event, which occurred on July 17, 1971. The offset displacements were measured at four stations by *King et al.* [1973, Figure 4] and were found to coincide closely to an elliptical curve. This is the shape of curve that would be predicted for the fault of Figure 1*b* with no net entrapped dislocation. In that case, when the origin of coordinates is placed at the center of the fault and when perturbations due to the breakdown zone are neglected, the elasticity solution for the offset displacement is (see, e.g., equations (22) and (96) of *Rice* [1968])

$$\delta = \delta_{max}[1 - x^2/(l/2)^2]^{1/2}$$
$$\delta_{max} = (1 - \nu)(\tau_a - \tau_F)l/G \tag{66}$$

The reported value of δ_{max} is 9 mm and $l = 6$ km. This corresponds to a very low driving stress; taking $\nu = 0.2$ and $G = 2 \times 10^4$ MN/m² (=2×10^5 bars) as representative, we compute $(\tau_a - \tau_F) = 0.38$ bars. If we reexpress the stress intensity factor from (3) in terms of δ_{max} and use (8), we obtain

$$K_{crit} = \frac{G\delta_{max}}{1-\nu}\left(\frac{\pi}{2l}\right)^{1/2}$$
$$\mathcal{G}_{crit} = \frac{1-\nu}{2G}K_{crit}^2 = \frac{\pi G\delta_{max}^2}{4(1-\nu)l} \quad (67)$$

and with the numerical values quoted above we compute $\mathcal{G}_{crit} = 2.6 \times 10^2$ N/m (=2.6 bars mm). It is interesting to note that this value corresponds to the lower range of fracture energies reported by *Husseini et al.* [1975], corresponding to the arrest of seismic slips on previously active faults.

The breakdown zone size ω is given by (16) in terms of the offset $\bar{\delta}$, at which breakdown is complete in Figure 2*b*, and of the stress drop $(\tau_B - \tau_F)$ from the inception of breakdown to residual sliding friction. Unfortunately, we have no direct experimental evidence to aid in the choice of either of these parameters, although since the cross-hatched area in Figure 3*b* is equal to $\mathcal{G}_{crit}$, the values to be chosen are constrained by

$$(\tau_B - \tau_F)\bar{\delta} \approx 2.6 \text{ bars mm} \quad (68)$$

We now consider some estimates of $\bar{\delta}$, which will allow us to estimate $(\tau_B - \tau_F)$ from this equation and hence to estimate ω from (16).

If we view the fault plane as rock surfaces in intimate mineral-to-mineral contact at asperities, where some degree of true adhesion occurs, we might then choose $\bar{\delta}$ as comparable in size to a true contact length. This we estimate as 10–100 μm (10^3 μm = 1 mm). With $\bar{\delta} = 10$ μm, $(\tau_B - \tau_F) = 260$ bars from (68), and (16) then leads to $\omega = 8$ mm. The figure based on the larger asperity size, namely, $\bar{\delta} = 100$ μm, leads to $(\tau_B - \tau_F) = 26$ bars and $\omega = 0.8$ m. The latter estimate is the basis of the value 1 m for ω chosen in our earlier calculations. In any case, ω/l should be very small, and if the smaller figure of $\omega = 8$ mm is more nearly correct, all observed creep events should correspond essentially to the curve labeled $\omega/l = 0$ in Figure 6, and the upper limit, beyond which seismic faulting ensues, would be given by $\mathcal{G}_{nom}/\mathcal{G}_{crit} = \beta^2$ (=1.77 for the value of β in Figure 6).

Alternatively, we might view the fault plane as consisting of a finely granulated rubble of particles ranging in size from claylike soil particles to sand and gravel. If $\bar{\delta}$ is identified as a representative particle size, the previous estimates of 10–100 μm and consequent estimates of ω might still be valid. On the other hand, we might proceed by viewing the gouge as a clay layer and by estimating $\bar{\delta}$ by comparison with the known values for virgin faulting of heavily overconsolidated clay soils presently at the earth's surface in the form of slopes or embankments. Indeed, PR noted that τ-δ curves for virgin failures of London clay specimens are consistent with $\bar{\delta}$ values in the range of 3–8 mm. But specimens which contain a previously slipped shear band show very little recovery of strength, and it would seem difficult to justify a $\bar{\delta}$ value for initiation of further slip as large as, say, 0.5 mm. If we take a $\bar{\delta}$ of 0.5 mm to correspond to an upper bound on the recovery of strength by some unspecified mechanism between slip events on a claylike fault gouge, this would lead to an upper bound to end zone size of $\omega = 19$ m and to $(\tau_B - \tau_F) = 5.2$ bars. This breakdown zone size is also much larger than the ones estimated in PR for virgin slip surface propagation in landslide failures of clay slopes, in which cases ω was found to lie in the range of one to a few meters.

It is clear from the foregoing that a definitive choice for ω cannot presently be made, and further experimental information is obviously needed. Fortunately, our comparison of representative creep event lengths and speeds with predictions in Figure 6 is not sensitively dependent on this choice. While the prediction of the instability velocity and the corresponding $\mathcal{G}_{nom}$ value does depend strongly on ω, our more general conclusion, that observed fault creep events are stabilized against rapid spreading by the fluid interaction effects discussed here, is little affected.

Slip Surface Propagation in the Progressive Landslide Failure of Overconsolidated Clay Slopes

We have alluded to the strong analogy between factors which could lead to the stabilization of earth faults against rapid spreading and those which could be responsible for the progressive failure of overconsolidated clay slopes. The phenomenology of the latter has been set forth by *Skempton* [1964] and *Bjerrum* [1967]: Owing to the unstably falling nature of the stress-deformation relation beyond peak strength, failure once initiated, say, by the notchlike stress concentration at the base of a slope, tends to localize as a narrow slip surface which propagates up the slope in a cracklike manner, and a final continuous rupture path forms which allows the downhill mass motion.

Because of the falling τ-δ relation, the shear resistance mobilized at any instant along the ultimate surface of rupture is highly nonuniform, and conventional 'limiting equilibrium' methods of slope stability analysis, based on a uniformly mobilized peak strength, tend often to overestimate slope stability [*Skempton*, 1964]. The PR model of slope failure as the propagation of a shear fault, subject to a τ-δ relation as in Figure 3*a*, seems to provide a suitable general framework for such failures, but no convincing explanation has been put forward for the time dependence of the failure process. Small progressive downslope mass motions are sometimes observed for periods ranging up to several years before a landslide. Also, even when failure takes place on a short time scale, say, immediately following an excavation cut, the failure propagation seems to be essentially quasi-static [*Bishop*, 1973].

As a possible factor leading to this time dependence it is noted that except in arid regions, such clay slopes will be fully saturated and hence, due to the high drained compressibility of the soil skeleton as compared to the individual compressibilities of its solid and liquid constituents, undrained response is essentially incompressible and $\nu_u = 0.5$. As was remarked in connection with Figure 4, this means that β is large, say, 1.7, and as was shown by the uppermost curve in Figure 4, the increasing resistance to rupture propagation with spreading speed is quite substantial. The maximum ratio of $\mathcal{G}_{nom}/\mathcal{G}_{crit}$ for this curve is $\beta^2 = 2.78$, although the ratio ω/l cannot be expected to be very small and the more detailed analysis in Figure 6 suggests that for $\omega/l \approx 0.01$ to 0.1, which might be taken as representative, the actual increase of $\mathcal{G}_{nom}/\mathcal{G}_{crit}$ above unity may be only $\frac{1}{4}$ or so of this value. Still, the predicted effect is large, and it could provide the mechanism of stabilization against rapid slip surface propagation.

The range of spreading speeds over which the effect is important is very different now, owing to the great difference in properties of clay as opposed to rock. We take a value of $c = 10^{-2}$ cm^2/s as representative for elastic behavior of clay; this corresponds to a permeability $k = 10^{-7}$cm/s and uniaxial drained compressibility $m_v = 10^{-2}$/bar, where we use the usual soil mechanics symbols [e.g., *Terzaghi*, 1943, chap. 13]. Also, we consider a slip surface length $l = 10$ m. From Figures 4 and 6 the plots of $\mathcal{G}_{nom}/\mathcal{G}_{crit}$ are steeply rising over the range of

Vl/c extending from, say, 1 to 100, and it may be assumed that over the corresponding range of spreading speeds, the coupled deformation-diffusion effect under consideration is active in stabilizing the growing slip surface against unstable propagation. With the assumed values of c and l we find this range of V to extend from approximately 3 m/yr to 1 m/d. These speeds do seem to be in a range consistent with the longer-term progressive slope failures, although not for failure times of the order of a day or so, and this mechanism of slope stabilization would seem to merit further study in the modeling of landslide phenomena.

Conclusion

We have demonstrated that the coupled deformation-diffusion processes in fluid-infiltrated porous solids lead to a mechanism which can account for the stabilization of fault spreading. The principal results are embodied in Figures 4 and 6 and the accompanying discussions. The comparison with observed creep events on the San Andreas fault system suggests that this may provide a viable mechanism for fault creep. Also, a possible relevance to long-term progressive failure of clay slopes has been indicated.

Here, for purposes of simply illustrating the phenomenon, attention has been limited to a simple plane strain fault geometry with steady state fault propagation. For further study of the mechanism it would seem appropriate to seek mathematical solutions for more general time histories of fault spreading (e.g., for a finite fault spreading from zero initial size at arbitrary speed) and for three-dimensional fault models, since the antiplane strain components of fault motion should be much less sensitive to these effects. In addition, as was remarked in the introduction, there are other factors which might contribute to the stabilization of fault spreading, and these would likewise merit further analysis.

Appendix

The solution to (18), (19), and (22) subject to boundary conditions (24)–(26) is developed here by Fourier transforms, defined so that any field variable f and its transform $\tilde{f}$ are related by

$$\tilde{f}(\kappa, y) = \int_{-\infty}^{+\infty} f(x, y)e^{-i\kappa x}\, dx \tag{A1a}$$

$$f(x, y) = \frac{1}{2\pi}\int_{-\infty}^{+\infty} \tilde{f}(\kappa, y)e^{i\kappa x}\, d\kappa \tag{A1b}$$

Application of (A1a) to (19) and (22) and elimination in the usual way of solutions which grow exponentially in y lead to

$$\begin{aligned}\tilde{\sigma}_{xx} + \tilde{\sigma}_{yy} + 2\eta\tilde{p} &= 2(1-\mu)A(\kappa)\exp[-m(\kappa)y] \\ \tilde{\sigma}_{xx} + \tilde{\sigma}_{yy} + (2\eta/\mu)\tilde{p} &= -[2(1-\mu)/\mu]B(\kappa) \\ &\quad \cdot \exp[-n(\kappa)y]\end{aligned} \tag{A2}$$

where the functions $A(\kappa)$, $B(\kappa)$ are yet to be determined and where

$$\begin{aligned} m^2(\kappa) &= \kappa^2 \qquad \mathrm{Re}\,[m(\kappa)] \geq 0 \\ n^2(\kappa) &= \kappa^2 - i\kappa V/c \qquad \mathrm{Re}\,[n(\kappa)] \geq 0\end{aligned} \tag{A3}$$

Here Re means 'real part of.' It is convenient to rewrite (A2), in abbreviated form, as

$$\begin{aligned}(\tilde{\sigma}_{xx} + \tilde{\sigma}_{yy})/2 &= Ae^{-my} + Be^{-ny} \\ \eta\tilde{p} &= -\mu Ae^{-my} - Be^{-ny}\end{aligned} \tag{A4}$$

After transformation the remaining field equations (18) can be rearranged in the form

$$\begin{aligned}-i\kappa(\tilde{\sigma}_{yy} - \tilde{\sigma}_{xx})/2 + \partial\tilde{\sigma}_{xy}/\partial y &= -i\kappa(\tilde{\sigma}_{xx} + \tilde{\sigma}_{yy})/2 \\ i\kappa\tilde{\sigma}_{xy} + \partial[(\tilde{\sigma}_{yy} - \tilde{\sigma}_{xx})/2]/\partial y &= -\partial[(\tilde{\sigma}_{xx} + \tilde{\sigma}_{yy})/2]/\partial y\end{aligned} \tag{A5}$$

The terms on the right side of these equations are expressible in terms of the first of (A4), and hence (A5) may be viewed as a coupled pair of first-order differential equations for the variables $(\tilde{\sigma}_{yy} - \tilde{\sigma}_{xx})/2$ and $\tilde{\sigma}_{xy}$. The homogeneous solution which does not grow exponentially with y is given by the pair

$$C(\kappa)\exp[-m(\kappa)y] \qquad [-i\kappa/m(\kappa)]C(\kappa)\exp[-m(\kappa)y]$$

where the function $C(\kappa)$ is also yet to be determined. To these we add particular solutions giving the proper right-hand side, and the results, in abbreviated notation, are

$$(\tilde{\sigma}_{yy} - \tilde{\sigma}_{xx})/2 = (C + myA)e^{-my} + [(\kappa^2 + n^2)/(\kappa^2 - n^2)]Be^{-ny} \tag{A6a}$$

$$\tilde{\sigma}_{xy} = -(i\kappa C/m + i\kappa yA)e^{-my} - [2i\kappa n/(\kappa^2 - n^2)]Be^{-ny} \tag{A6b}$$

These, together with (A4), determine transforms of all the field variables in terms of the three unknown functions A, B, C, which must, in turn, be chosen to satisfy the boundary conditions, (24)–(26). The first two sets of boundary conditions require that p and σ_{yy} vanish on the entire x axis. So also must their transforms, and thus

$$\begin{aligned}\mu A(\kappa) + B(\kappa) &= 0 \\ A(\kappa) + \{2\kappa^2/[\kappa^2 - n^2(\kappa)]\}B(\kappa) + C(\kappa) &= 0\end{aligned} \tag{A7}$$

The remaining boundary conditions give σ_{xx} for $x > 0$ and σ_{xy} for $x < 0$. Thus the transforms $\tilde{\sigma}_{xx}$ and $\tilde{\sigma}_{xy}$ are incompletely specified, and these boundary conditions reduce to

$$A(\kappa) - \{2n^2(\kappa)/[\kappa^2 - n^2(\kappa)]\}B(\kappa) - C(\kappa) = G^+(\kappa) \tag{A8a}$$

and

$$-\{2i\kappa n(\kappa)/[\kappa^2 - n^2(\kappa)]\}B(\kappa) - [i\kappa/m(\kappa)]C(\kappa) = F^-(\kappa) - \tilde{\tau}(\kappa) \tag{A8b}$$

where

$$\tilde{\tau}(\kappa) = \int_{-\infty}^{0} \tau(x)e^{-i\kappa x}\, dx \tag{A9a}$$

$$\begin{aligned}G^+(\kappa) &= \int_{-\infty}^{0} \sigma_{xx}(x, 0)e^{-i\kappa x}\, dx \\ F^-(\kappa) &= \int_{0}^{\infty} \sigma_{xy}(x, 0)e^{-i\kappa x}\, dx\end{aligned} \tag{A9b}$$

Viewed as equations for A, B, and C, (A7)–(A8) are overdetermined and may be solved only if a certain consistency relation is satisfied by the further unknown functions G^+ and F^-. This consistency relation, together with the fact that G^+ and F^- are analytic in the upper and lower portions, respectively, of the complex κ plane, as suggested by the superscripts, suffices (in principle) to determine them and hence A, B, C,

and the transforms of all the σ's and p, by the Wiener-Hopf method [see *Noble*, 1958].

The details of the solution are now carried out for the shear loading function $\tau^{(\lambda)}(x)$ of (27). When reported in the main part of the text, functions A, B, C, σ_{ij}, etc., corresponding to this loading will be given the superscript (λ). From (A7) and the first of (A8),

$$A(\kappa) = G^+(\kappa)/[2(1-\mu)]$$
$$B(\kappa) = -\mu G^+(\kappa)/[2(1-\mu)] \qquad \text{(A10)}$$
$$C(\kappa) = -(1 + 2ic\mu\kappa/V)G^+(\kappa)/[2(1-\mu)]$$

When these are substituted into the second of (A8) there results the consistency condition

$$\{i\kappa/m(\kappa) + (2\mu c/V)[n(\kappa) - m(\kappa)]\} \cdot G^+(\kappa)/[2(1-\mu)] = F^-(\kappa) - \tilde{\tau}(\kappa) \qquad \text{(A11)}$$

Now we write $\tau(x) = e^{i\lambda x}$ in (A9a), where it is understood that λ has a small negative imaginary part whenever required for convergence or the elimination of ambiguity, and obtain

$$\tilde{\tau}(\kappa) = 1/[i(\lambda - \kappa)] \qquad \text{(A12)}$$

As derived, (A11) holds only on the real κ axis. Our aim, however, in the Wiener-Hopf technique is to rewrite it in a form for which every function which appears is analytic in some upper or lower half plane and for which every function which appears shares some common domain of analyticity.

We note that $n(\kappa)$ and $m(\kappa)$ can be written in the form

$$m(\kappa) = m^+(\kappa)m^-(\kappa) \qquad n(\kappa) = m^+(\kappa)\, n^-(\kappa) \qquad \text{(A13)}$$

where

$$m^+(\kappa) = \kappa^{1/2} \qquad m^-(\kappa) = (\kappa - i\epsilon)^{1/2}$$
$$n^-(x) = (\kappa - iV/c)^{1/2} \qquad \text{(A14)}$$

and where ϵ is a small positive constant which ultimately will be allowed to vanish. The branch cut for m^+ is the entire negative imaginary κ axis, whereas the ones for m^- and n^- lie on the positive imaginary axis from the points $i\epsilon$ and iV/c, respectively, to $i\infty$. Thus the superscripts plus or minus again denote the region of the κ plane where a function is analytic. We note also the identity $\kappa = [m^+]^2 = [m^-]^2$.

Substituting (A12) into (A11) and rearranging in accord with our goals yield

$$-\frac{G^+(\kappa)}{2im^+(\kappa)} - \frac{1}{i(\kappa-\lambda)m^-(\lambda)D^-(\lambda)} = \frac{F^-(\kappa)}{m^-(\kappa)D^-(\kappa)} + \frac{1}{i(\kappa-\lambda)}\left[\frac{1}{m^-(\kappa)D^-(\kappa)} - \frac{1}{m^-(\lambda)D^-(\lambda)}\right] \qquad \text{(A15)}$$

where

$$(1-\mu)D^-(\kappa) = 1 + (2i\mu\kappa c/V)\,[1 - n^-(\kappa)/m^-(\kappa)] \qquad \text{(A16)}$$

As suggested by the notation, the function $D^-(\kappa)$ is analytic and free of zeros in the lower half κ plane and in fact for Im $(\kappa) < \epsilon$, and it tends to a finite value as $\kappa \to \infty$. Thus whereas the left side of (A15) is analytic in the upper half plane Im $(\kappa) > 0$, the right side is analytic in the lower half plane Im $(\kappa) < \epsilon$.

Thus since the two sides of (A15) share a common domain of analyticity, they must be analytic continuations of one another, so that both the right side and the left side can be equated to another function, say, $H(\kappa)$, which is analytic in the entire κ plane. In order to determine this function, the properties of both sides of (A15) must be investigated for $\kappa \to \infty$. By observation of the definition of $G^+(\kappa)$ and $F^-(\kappa)$ in (A9b), we can assert that both sides of (A15) approach zero as $\kappa \to \infty$ in their respective domains of analyticity. Thus by Liouville's theorem, $H(\kappa)$ must vanish identically.

This means that both sides of (A15) must vanish. We can then write the solution

$$G^+(\kappa) = -2m^+(\kappa)/[(\kappa - \lambda)m^-(\lambda)D^-(\lambda)] \qquad \text{(A17)}$$

and by inserting this into (A10), obtain the solution for the functions $A(\kappa)$, $B(\kappa)$, and $C(\kappa)$.

The above solution is used to write (28) in the main text and, through the superposition procedure of (31)–(33), to solve the problem of uniform shear loading (equations (34)–(41)).

Later in the text a solution is needed for the displacement field corresponding to $\tau^{(\lambda)}(x)$. To obtain this, note that by the stress-strain relations (17a) with condition of plane strain and the boundary condition (25), we have

$$\epsilon_{xx}(x, 0) = (1-\nu)\sigma_{xx}(x, 0)/(2G) \qquad \text{(A18)}$$

If u_x is the displacement of the upper fault surface in the x direction, we may write $\epsilon_{xx} = \partial u_x/\partial x$ and note also from the antisymmetry that the total slip offset can be written as $\delta = 2u_x$. Thus

$$\delta(x) = [(1-\nu)/G]\int_0^x \sigma_{xz}(x, 0)\, dx \qquad x < 0 \qquad \text{(A19)}$$

Using the solution above and noting (A9b), we have for the shear loading $\tau^{(\lambda)}(x)$

$$\tilde{\sigma}_{xx}{}^{(\lambda)}(\kappa, 0) = G^{+(\lambda)}(\kappa) = -2m^+(\kappa)/[(\kappa - \lambda)m^-(\lambda)D^-(\lambda)] \qquad \text{(A20)}$$

where now the superscript (λ) is attached as in the main text. Thus by Fourier inversion,

$$\delta^{(\lambda)}(x) = \frac{1-\nu}{G}\int_0^x \left\{\frac{1}{2\pi}\int_{-\infty}^{+\infty} G^{+(\lambda)}(\kappa)e^{i\kappa z}\, d\kappa\right\} dx = \frac{1-\nu}{i\pi G m^-(\lambda)D^-(\lambda)}\int_{-\infty}^{+\infty}\frac{1-e^{i\kappa x}}{m^+(\kappa)(\kappa-\lambda)}\, d\kappa \qquad \text{(A21)}$$

To evaluate this, it is simplest to multiply both sides by $e^{-i\lambda x}$, differentiate with respect to x, then shift the path to one which wraps around the branch cut for $m^+(\kappa)$ along the negative imaginary axis, and finally integrate both sides from $x = 0$ to some general point $x < 0$. The final result is

$$\delta^{(\lambda)}(x) = \frac{2(1-\nu)e^{i\lambda x}\ \text{erf}\,[e^{-i\pi/4}m^-(\lambda)\,|x|^{1/2}]}{G\lambda D^-(\lambda)} \qquad \text{(A22)}$$

where $\text{erf}\,(\xi) = (2/\pi^{1/2})\int_0^\xi e^{-\eta^2}\, d\eta$. This solution is used with the superposition formalism to obtain (50)–(54) of the main text.

Acknowledgments. This study was supported by NSF grant GA-43380 and by Brown University. We are grateful to M. P. Cleary for helpful discussions.

REFERENCES

Anderson, D. L., and J. H. Whitcomb, Time-dependent seismology, *J. Geophys. Res., 80*, 1497–1503, 1975.

Biot, M. A., General theory of three-dimensional consolidation, *J. Appl. Phys., 12*, 155–164, 1941.

Bishop, A. W., Discussion, in *Plasticity and Soil Mechanics*, edited by A. C. Palmer, pp. 295–296, Cambridge University Engineering Department, Cambridge, England, 1973.

Bjerrum, L., Progressive failure in slopes of overconsolidated plastic clay and clay shales, *Trans. Amer. Soc. Civil Eng., SM93*, 3–49, 1967.

Husseini, M. E., D. B. Jovanovich, M. J. Randall, and L. B. Freund, The fracture energy of earthquakes, *Geophys. J. Roy. Astron. Soc., 43*, 367–385, 1975.

Irwin, G. R., Fracture mechanics, in *Structural Mechanics*, edited by J. N. Goodier, and N. J. Hoff, pp. 557–592, Pergamon, New York, 1960.

Johnson, A. G., R. L. Kovach, and A. Nur, Fluid-pressure variations and fault creep in central California, *Tectonophysics, 23*, 257–266, 1974.

King, C-Y., R. D. Nason, and D. Tocher, Kinematics of fault creep, *Phil. Trans. Roy. Soc. London, Ser. A, 274*, 355–360, 1973.

Nason, R., and J. Weertman, A dislocation theory analysis of fault creep events, *J. Geophys. Res., 78*, 7745–7751, 1973.

Noble, B., *Methods Based on the Wiener-Hopf Technique*, Pergamon, New York, 1958.

Palmer, A. C., and J. R. Rice, The growth of slip surfaces in the progressive failure of overconsolidated clay, *Proc. Roy. Soc. London, Ser. A, 332*, 527–548, 1973.

Paris, P. C., and G. C. Sih, Stress analysis of cracks, in *Fracture Toughness Testing and Its Applications, Spec. Tech. Publ. 381*, pp. 30–76, American Society of Testing and Materials, Philadelphia, Pa., 1965.

Rice, J. R., Mathematical analysis in the mechanics of fracture, in *Fracture: An Advanced Treatise*, vol. 2, edited by H. Liebowitz, pp. 191–311, Academic, New York, 1968.

Rice, J. R., The initiation and growth of shear bands, in *Plasticity and Soil Mechanics*, edited by A. C. Palmer, pp. 263–274, Cambridge University Engineering Department, Cambridge, England, 1973.

Rice, J. R., and M. P. Cleary, Some basic stress diffusion solutions for fluid-saturated elastic porous media with compressible constituents, *Rev. Geophys. Space Phys., 14*(2), 227–241, 1976.

Scholz, C. H., Mechanism of creep in brittle rocks, *J. Geophys. Res., 73*, 3295–3302, 1968.

Scholz, C. H., M. Wyss, and S. W. Smith, Seismic and aseismic slip on the San Andreas fault, *J. Geophys. Res., 74*, 2049–2069, 1969.

Skempton, A. W., Long term stability of clay slopes, *Geotechnique, 14*, 77–101, 1964.

Terzaghi, K., *Theoretical Soil Mechanics*, chap. 13, p. 272, Wiley, New York, 1943.

(Received December 17, 1975;
revised May 24, 1976;
accepted May 27, 1976.)